MR imaging of acute spinal cord trauma.

D W Chakeres, F Flickinger, J C Bresnahan, M S Beattie, K L Weiss, C Miller and B T Stokes

AJNR Am J Neuroradiol 1987, 8 (1) 5-10
http://www.ajnr.org/content/8/1/5

MR Imaging of Acute Spinal Cord Trauma

Donald W. Chakeres[1]
Fred Flickinger[1]
Jacqueline C. Bresnahan[2]
Michael S. Beattie[2,3]
Kenneth L. Weiss[1]
Carol Miller[3]
Bradford T. Stokes[4]

The thoracic spinal cords of five mongrel dogs were imaged with a 1.5 T MR scanner before and after trauma induced by a well-established method of spinal cord impaction that produces central cord hemorrhagic necrosis. The anesthetized dogs were studied acutely with a 5-in. circular surface coil, 12-cm field of view, sagittal and axial partial-saturation (TR = 600, TE = 25 msec) and spin-echo (TR = 2000, TE = 25–100 msec) techniques. One normal dog was used as a control. The cords were surgically removed and histologically examined. Direct correlation of the pathologic findings and imaging data showed that at the level of trauma there was obliteration of epidural fat and CSF spaces secondary to central cord hemorrhage and edema. The traumatized cords expanded to fill the bony canal, and there was loss of visualization of the internal anatomy of the cord (gray- and white-matter structures). We conclude that MR can accurately identify cord hemorrhage and edema within a few hours of spinal trauma.

Each year in the United States there are approximately 10,000 new cases of traumatic spinal cord injuries. The majority of these occur in young people. The imaging techniques currently used to diagnose spinal cord injury include plain radiographs, tomography, CT, and myelography [1–3]. Unfortunately, these techniques usually provide only indirect evidence of spinal cord injury, such as status of the vertebral alignment, presence and location of osseous fracture fragments relative to the spinal canal, overall dimension and configuration of the spinal cord, and patency of the spinal subarachnoid space. Occasionally, after metrizamide myelography, metrizamide can be seen penetrating the cord [2]. Cord edema can also be detected as focal enlargement. None of these techniques provides a direct image of the nature or extent of cord damage, since the internal anatomy of the spinal cord cannot be visualized. Thus, evaluation must be primarily clinical rather than radiographic. Therapy is limited to systemic corticosteroids, preventive positioning (traction), and surgical decompression for spinal cord compression or hemorrhage.

The lack of a noninvasive examination to evaluate the extent and type of spinal cord trauma has forced reliance on animal autopsy studies or follow-up physiologic testing to study the effects of spinal cord trauma [4]. Evaluation of treatment has also been hindered since there are no accurate radiologic tests to predict the extent of injury.

MR has been shown to be an excellent technique for identifying a wide range of abnormalities of the spinal cord, including syrinx, neoplasm, hemorrhage, edema, and congenital anomalies [5, 6]. This study was designed to evaluate the utility of MR in identifying the presence and extent of acute spinal cord trauma in dogs.

Materials and Methods

Five mongrel dogs ranging in weight from 4.5–11.3 kg (mean, 7.8 kg) were used for this study. Each dog was initially anesthetized with chloralose (5 mg/kg) and urethane (35 mg/

Received January 29, 1986; accepted after revision July 9, 1986.

Presented at the annual meeting of the American Society of Neuroradiology, San Diego, January 1986.

This work was supported in part by grants from the National Institute of Health NS-10165 and the Magnetic Resonance Imaging Operating Panel of the Ohio State University, Columbus, OH.

[1] Department of Radiology, Ohio State University College of Medicine, Ohio State University Hospital, 410 W. 10th Avenue, Columbus, OH 43210. Address reprint requests to D. Chakeres.

[2] Department of Anatomy, Ohio State University College of Medicine, Ohio State University Hospital, Columbus, OH 43210.

[3] Department of Surgery, Division of Neurosurgery, Ohio State University College of Medicine, Ohio State University Hospital, Columbus, OH 43210.

[4] Department of Physiology, Ohio State University College of Medicine, Ohio State University Hospital, Columbus, OH 43210.

AJNR 8:5–10, January/February 1987
0195-6108/86/0801-0005

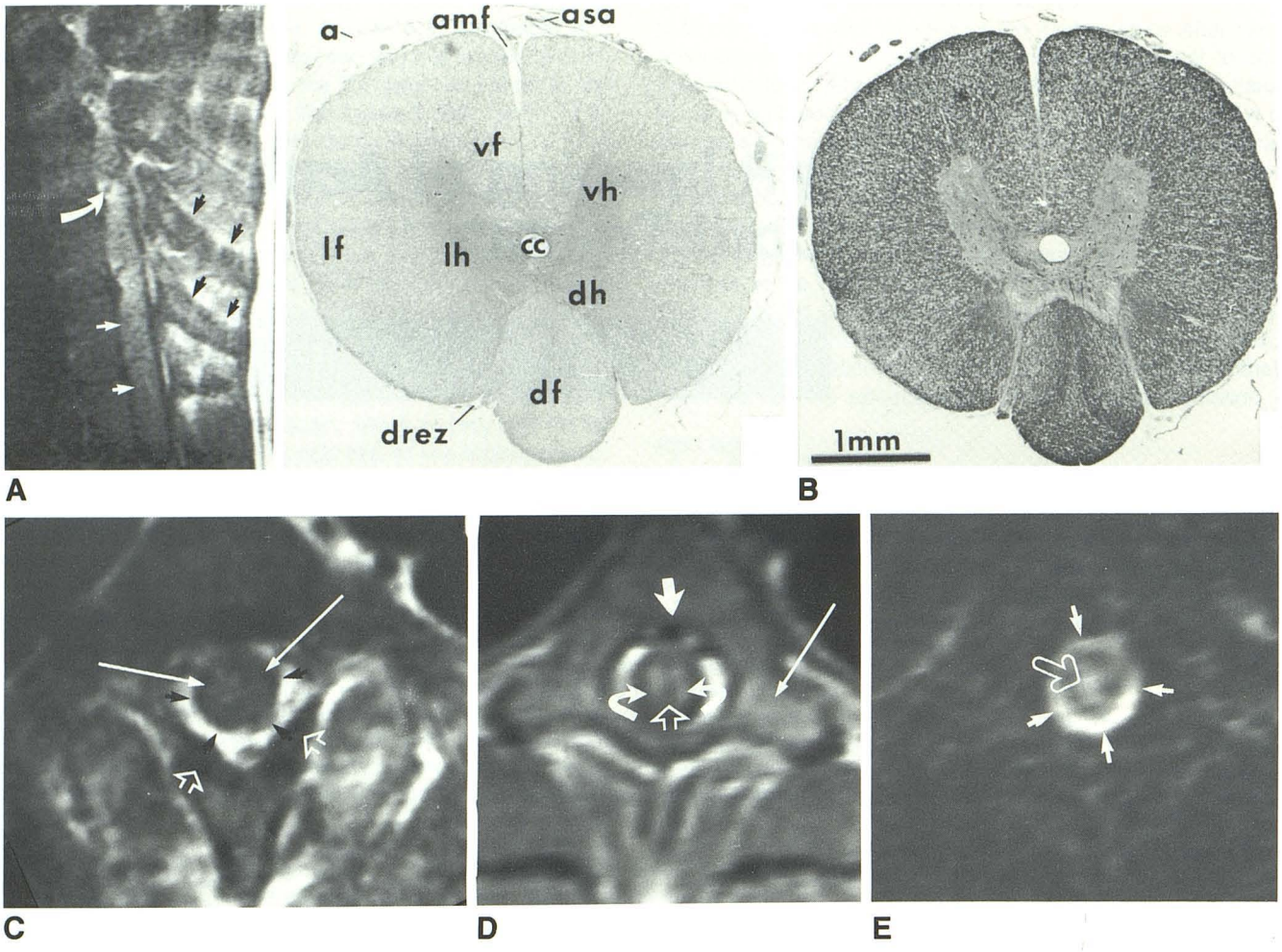

Fig. 1.—*A*, Normal sagittal spine, prelaminectomy. Spinal cord (*straight white arrows*) is seen on this localizer 5-mm-thick sagittal partial-saturation TR = 600, TE = 25 msec image. Note fat planes between spinous processes (*black arrows*) and epidural fat surrounding nerve root (*white curved arrow*).

***B*, Normal histology of thoracic cord. Two histologic axial sections of mid-thoracic spinal cord. Left-hand section is stained with H and E. Right-hand section is stained for myelin with Luxol Fast Blue and for cell bodies with Cresyl echt violet. Labeled structures include anterior spinal artery (asa), anterior median fissure (amf), central canal (cc), arachnoid membrane (a), dorsal funiculus (df), dorsal horn (dh), dorsal root entry zone (drez), lateral funiculus (lf), ventral horn (vh), lateral horn (lh), and ventral funiculus (vf).**

***C*, Outer surface of thoracic spinal cord (*long white arrows*) is seen on this axial partial-saturation TR = 600, TE = 25 msec image. Lower signal intensity CSF (*black arrows*) is interposed between cord and intense epidural fat. Low-intensity lamina (*open white arrows*) are labeled.**

***D*, We suspect that gray matter is seen as an intermediate-intensity circle (*curved arrows*) with a central vertical cleft (*open arrowhead*) on this axial spin-echo TR = 2000, TE = 25 msec image. Epidural fat is seen as two high-signal crescents. Cortical bone adjacent to epidural fat is low-signal, while marrow spaces, such as in transverse process (*long thin arrow*) are intense. An epidural vein (*thick arrow*) in anterior canal is also visible.**

***E*, High-signal CSF ring (*solid white arrows*) about spinal cord remains intense on this axial TR = 2000, TE = 100 msec spin-echo image. *Open white arrow* is directed toward central cord.**

kg) administered intravenously with supplemental doses given to maintain deep anesthesia for the duration of the experiment. This anesthesia has been shown to induce no changes (such as edema) in the central nervous system [7]. After sedation, the first (control) dog was imaged with a 1.5-T General Electric MR imaging system. A prototype receive-transmit 5-in.-diameter circular surface coil was placed under the dog's spine and centered at the midthoracic level. Sagittal 5-mm localizing partial saturation (TR = 600, TE = 25 msec) images were made with a field of view of 12 cm (Fig. 1). Axial 5-mm spin-echo images were obtained with a TR of 2000 msec, two averages, TEs of 25, 50, 75, 100 msec, and a pixel matrix of 128 × 256. Partial-saturation images with TR = 600 and TE = 25 msec were also made with a matrix of 256 × 256 (Fig. 1). The same techniques were used for each imaging sequence.

A single-level laminectomy was then performed at approximately the sixth thoracic level. The epidural fat was aspirated by suction to expose the dura. Care was taken not to injure the spinal cord, and the surgical site was packed with dressings to ensure hemostasis. The dog was returned to the MR facility and imaged 2 and 4 hr after laminectomy using the previous techniques. After the surgical site was recognized by a sagittal localizing image (Fig. 2A), the region of laminectomy was imaged in the identical axial fashion as presurgically (Fig. 2B).

The next four dogs were studied postlaminectomy, pretrauma to

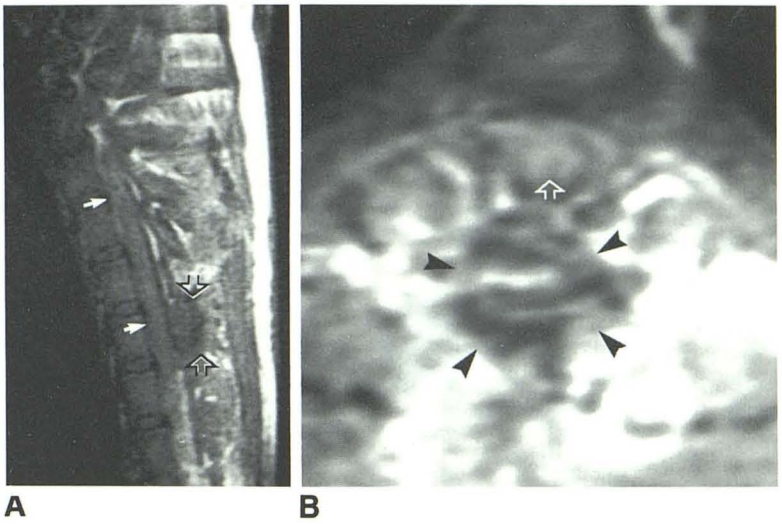

Fig. 2.—*A*, Postlaminectomy, pretrauma. Surgical site (*open arrows*) is seen on this axial TR = 600, TE = 25 msec partial-saturation sagittal image. Distortion of posterior elements by surgery and packing is seen. Spinal cord (*solid arrows*) is unaffected.

***B*, This 5-mm-thick TR = 2000, TE = 25 msec axial image obtained after laminectomy (*black arrowheads*), pretrauma, shows that internal anatomy of cord is unchanged. The apparent central cleft of spinal cord is still visible (*open white arrow*).**

provide another control set of images. The dogs were returned to the laboratory for spinal cord injury using the classical weight-drop technique described by Allen [8]. A 20-g weight was dropped 20 cm down a vented tube onto the exposed dura. The tube was held in a stereotaxic device that was positioned over the spinal cord. The T5 and T7 spinous processes were secured to a spinal frame to reduce movement of the spinal cord due to respiration during the impact. This type of injury to the spinal cord produces profound functional deficits in dogs [9]. The dogs were subsequently imaged 2–4 hr after spinal cord injury. The control dog and the first dog with spinal cord injury were sacrificed by anesthetic overdose, and the region of the spinal cord studied by MR was removed and immersion-fixed in 10% formalin. The other three dogs were sacrificed by intracardiac perfusion with saline followed by 10% formalin 4–5 hr posttrauma. The spinal cords were surgically removed and placed in 10% formalin for 2–5 weeks. All cords were embedded in paraffin, sectioned at 20 μm intervals, and every 10th and 11th section through the lesion was stained for Nissl and Luxol Fast Blue or H and E, respectively. Representative sections of the lesion were drawn and compared with the MR images (Figs. 1 and 3).

Results

In normal dogs the spinal cord measurement varies with the dog's size. The outer dimensions of all normal spinal cords at the midthoracic level were between 4–5 mm in diameter (Fig. 1). The gray-matter structures span a total diameter of 2.5 mm and form a "butterfly" shape within the central cord.

The control dog's spinal cord before surgery and without trauma (Fig. 1) almost filled the dural sac. The sagittal and axial partial-saturation TR = 600, TE = 25 msec images showed the outer margins of the intermediate signal thoracic cord outlined by low-signal-intensity CSF. The epidural fat was most intense. The axial spin-echo images were more informative, since the internal anatomy of the spinal cord could be identified (Fig. 1D and 1E). A "butterfly" shaped region conforming to the gray-matter structures was visible on the axial spin-echo (TR = 2000, TE = 25 msec) images (Fig. 1D). The epidural fat and bone marrow were seen as high-signal regions about the subarachnoid space on the short TE spin-echo and partial-saturation images (25 msec) (Fig. 1C and 1D). The later spin-echo images (TE = 75 and 100 msec, TR = 2000 msec) demonstrated a high-signal "donut" appearance of the CSF (Fig. 1E).

A number of imaging aberrations can occur with MR that are not seen with CT. We have seen apparent clefts in small solid phantoms probably related to Fourier transformation artifacts. These types of changes are more visible in the phase-encoding axis when the matrix is 128 compared with the 256 matrix frequency-encoded axis. Because of this, it is possible that some of the findings related to the internal anatomy of the spinal cord are partially artifactual.

The surgical site was visible because the normal posterior elements and epidural fat were absent and replaced with amorphous packing material (Fig. 2). The packing had a high intensity on the TR = 2000, TE = 75,100 msec spin-echo images. After laminectomy, the spinal cord structures did not change in appearance. The anatomic findings, such as the visualization of the outer margin and the central gray matter of the spinal cord (Fig. 2B), were stable. The second series of images, done 4 hr after laminectomy on the control dog without trauma, did not change and neither did the postlaminectomy, pretrauma findings in the other group of dogs.

The histologic evaluation of the traumatized spinal cords showed petechial hemorrhage in the white matter (Fig. 3) as well as central hemorrhagic necrosis. The MR findings of the spine after trauma were similar for each traumatized dog. Above and below the laminectomy-trauma site the spinal structures were unaffected. At the level of the laminectomy and trauma, there was near complete obliteration of the CSF and epidural spaces, and internal and external anatomy of the normal spinal cord were not visible. The spinal canal itself was seen to be filled with a slightly inhomogeneous soft-tissue intensity. Axial views were essential to recognize these changes since they could not be seen on sagittal sections.

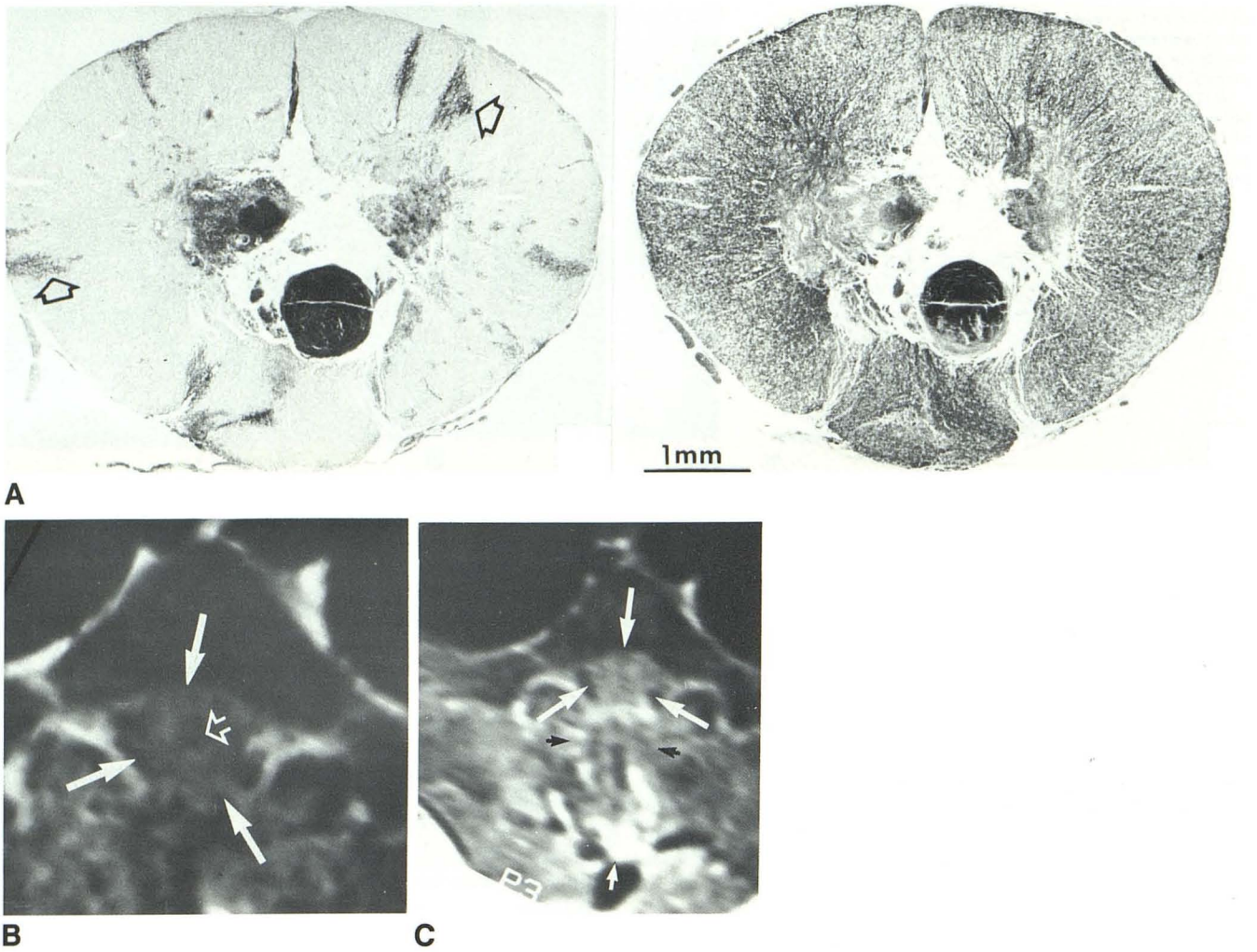

Fig. 3.—*A*, Posttrauma histology of cord. Central hemorrhagic necrosis and initial cavity formation are seen on this axial histologic section. Petechial hemorrhages (*arrows*) may be observed in white matter in H and E stained section (*left*). The integrity of white matter at this early time posttrauma (4 hr) is seen in the Luxol Fast Blue/Nissl-stained section (*right*).

B, Same thoracic level as in *A* is shown here using an axial partial-saturation technique (TR = 600, TE = 25 msec). Note that normal CSF spaces and spinal cord structures cannot be identified within spinal canal (*solid arrows*). Small central low-signal area (*open arrow*) may correspond to necrosis.

C, Posttrauma MR images. Same dog as in *A* and *B*, this axial spin-echo image shows obliteration of normal epidural, CSF spaces, and internal cord anatomy (TR = 2000, TE = 25 msec). Note slightly inhomogeneous appearance of contents of spinal canal (*large arrows*). Surgical site is marked by *small arrows*.

Discussion

There is currently no adequate imaging technique that directly evaluates spinal cord trauma. If a noninvasive examination were available, earlier diagnosis of a significant cord injury would be possible. This could have a significant impact on patient care, since appropriate intervention could follow without exposing the patient to the delays, risks, and complications associated with myelography or other radiographic procedures. Frequently, there is a discrepancy between the radiographic and clinical findings, so that treatment must be monitored by symptom status rather than radiographic findings. This study was performed to determine whether MR can be used to evaluate patients with acute traumatic spinal cord injury.

Laboratory studies of dogs and primates have shown that damage to the spinal cord after impaction trauma is similar to that seen in humans [4, 8, 10–14]. This type of cord injury simulates cord contusions such as those seen in crush injuries following diving or motor vehicle accidents.

The histologic and gross findings of acute blunt injury are characteristic in both humans and dogs. The extent of the injury depends on the amount of force of the trauma. Hemorrhage and edema within the central cord occur at the level of impact [7, 15, 16] and persists. Vascular disruption results in petechial hemorrhages, reduction in blood flow, and alteration of the blood-brain barrier [12, 17–19]. The spinal cord swells at the trauma site and can extrude through a defect in the dura, if the dura is torn. A football-shaped cavitation within the cord is seen [14, 20]. Central necrosis of the cord follows

over a period of hours to days [10, 20]. Degeneration of the white-matter tracts continues over a period of weeks [11–14]

The correlation between our MR results and the pathologic findings were good. Before trauma we were able to confidently visualize all the major structures within and about the spinal cord, even though they measured only a few millimeters in size. A series of concentric circles of diminishing diameter related to the cortical bone, epidural fat, CSF, and the cord structures were seen (Fig. 1). A combination of section planes and pulse-sequence techniques was needed for complete evaluation of the cord. The sagittal partial-saturation images were adequate for localizing the level of laminectomy but were not adequate to identify the spinal cord trauma. This is related primarily to the effects of partial volume averaging, since the voxels are filled by multiple tissues rather that just a single one. The axial sections are oriented so that the voxels are parallel to the spinal cord, epidural fat, and CSF. The partial-saturation images best demonstrated the relation of the CSF spaces to the outer surface of the cord on the axial sections.

On the axial spin-echo images (TR = 2000, TE = 25–100 msec) the outer contour of the spinal cord could not be seen well. The white-matter tracts have a lower proton density than the gray-matter structures [21]. This is similar to what is seen intracranially, where the white-matter tracts are of lower signal intensity than the gray-matter structures. The first echo (25 msec) clearly demonstrated the central gray matter of the cord. An oval region measuring about 2.5 mm in diameter with a central fissure was seen (Fig. 1D).

Following trauma, all the landmarks seen on the normal studies were absent (Figs. 3 and 4). We believe that these findings are secondary to expansion of the cord, which displaces the epidural fat and CSF from the spinal canal at the level of trauma. The edema and hemorrhage within the cord distorted the normal tracts so that they were not visible. The slightly inhomogeneous appearance to the spinal canal contents was probably related to the varying foci of hemorrhage and injured cord. The pixel size of 0.47 × 0.94 mm approaches the size of the individual hemorrhages (Fig. 3A). Acute hemorrhage usually has a signal similar to normal neural tissues at lower field strengths [22]. At higher field strengths acute hemorrhage may show a decreased signal [23]; however, subacute hemorrhage is usually quite intense on most pulse sequences. A dark halo can be seen at the periphery of chronic hemorrhage.

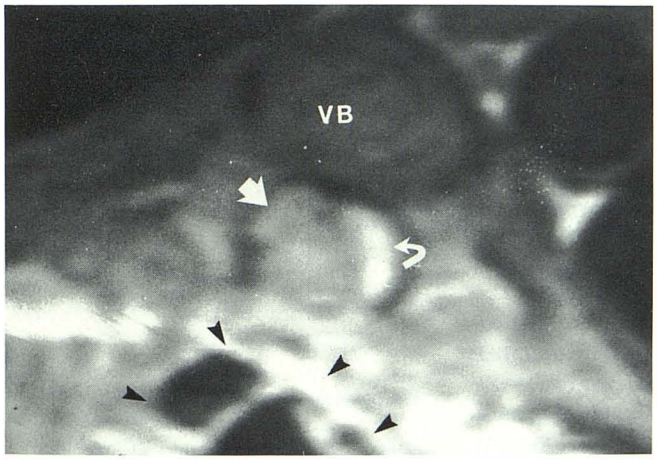

Fig. 4.—Posttrauma epidural distortion. This axial partial-saturation TR = 600, TE = 25 msec image from another postlaminectomy, posttrauma dog shows asymmetric epidural fat (normal side, *curved arrow*; pathologic side, *straight arrow*). Vertebral body (VB) and surgical site (*black arrowheads*) are labeled.

REFERENCES

1. Donovan Post MJ, Green BA, Quencer RM, Stokes NA, Callahan RA, Eismont FJ. The value of computed tomography in spinal trauma. *Spine* **1982**;7:417–431
2. Cooper PR, Cohen W. Evaluation of cervical spinal cord injuries with metrizamide myelography-CT scanning. *J Neurosurg* **1984**;61:281–289
3. Kassel E, Cooper PW, Rubenstein J. Radiology of spinal trauma: practical experience in a trauma unit. *J Can Assoc Radiol* **1983**;34:189–203
4. De La Torre JC. Spinal cord injury: review of basic and applied research. *Spine* **1981**;6:315–335
5. Norman D, Mills CM, Brant-Zawadzki M, Yeates A, Crooks LE, Kaufman L. Magnetic resonance imaging of the spinal cord and canal: potentials and limitations. *AJNR* **1983**;141:1147–1152
6. Hyman RA, Edwards JH, Vacirca SJ, Stein HL. 0.6 T MR imaging of the cervical spine: multislice and multiecho techniques. *AJNR* **1985**;6:229–236
7. Clendenon N, Gordon W, Allen J. Experimental spinal cord trauma: early alterations in fluid and electrolyte levels. *Neurosci Abstr* **1981**;7:87
8. Allen AR. Surgery of experimental lesion of spinal cord equivalent to crush injury of fracture dislocation of spinal column. *JAMA* **1911**;57:878–880
9. Albin M, White R, Locke GE, Massopust L, Kretchmer H. Localized spinal cord hypothermia—anaesthetic effects and application to spinal cord injury. *Anesth Analg* **1967**;46:8–16
10. Balentine JD. Pathology of experimental spinal cord trauma I: the necrotic lesion as a function of vascular injury. *Lab Invest* **1978**;39:236–253
11. Balentine JD. Pathology of experimental spinal cord trauma II: ultrastructure of axons and myelin. *Lab Invest* **1978**;39:254–265
12. Blight AR. Axonal physiology of chronic spinal cord injury in the cat: intracellular recording in vitro. *Neuroscience* **1983**; 10(4):1471–1486
13. Bresnahan JC. An electron microscopic analysis of axonal alterations following blunt contusions of the spinal cord of the Rhesus monkey (*Macaca mulatta*). *J Neurol Sci* **1978**;37:59–82
14. Bresnahan JC, King JS, Martin GF, Yashon D. A neuroanatomical analysis of spinal cord injury in the Rhesus monkey (*Macaca mulatta*). *J Neurol Sci* **1976**;28:521–542
15. St. Nemecek R, Suba P, Rozsival V, Melka O. Longitudinal extension of edema in experimental spinal cord injury: evidence for two types of post-traumatic oedema. *Acta Neurochir* **1977**;37:7–16
16. Green B, Wagner F. Evolution of edema in the acutely injured spinal cord: a fluorescence microscopic study. *Surg Neurol* **1973**;1:98–101
17. Bingham W, Goldman H, Friedman S, Murphy S, Yashon D, Hunt W. Blood flow in normal and injured monkey spinal cord. *J Neurosurg* **1975**;43:162–171
18. Dohrmann GJ, Wick KM, Bucy PC. Spinal cord blood flow

patterns in experimental traumatic paraplegia. *J Neurosurg* **1973**;38:52–58
19. Goodman J, Bingham G, Hunt W. Ultra-structural blood-brain barrier alterations and edema formation in acute spinal cord trauma. *J Neurosurg* **1976**;44:418–424
20. Kao C, Chang L, Bloodworth J. The mechanism of spinal cord cavitation following spinal cord transection. Part 2: electron microscopic observations. *J Neurosurg* **1977**;46:745–766
21. Wehrli FW, MacFal JR, Glover GH, Grigsby N. The dependence of nuclear magnetic resonance (NMR) image contrast on intrinsic and pulse sequence timing parameters. *Magn Res Imaging* **1984**;2:3–16
22. Chakeres DW, Bryan RN. Acute subarachnoid hemorrhage: in vitro comparison of magnetic resonance and computed tomography, *AJNR* **1986**;7:223–228
23. Gomori JM, Grossman RI, Goldberg HI, Zimmerman RA, Bilaniuk LT. Intracranial hematomas: imaging by high-field MR. *Radiology* **1985**;157:87–93